

# **Shigella promotes major alteration of gut epithelial physiology and tissue invasion by shutting off host intracellular transport**

Mariana Ferrari, Valérie Malardé, Laura Salavessa, Giulia Nigro, Stéphane Descorps-Declère, John Rohde, Pamela Schnupf, Vanessa Masson, Guillaume Arras, Damarys Loew, et al.

► **To cite this version:**

Mariana Ferrari, Valérie Malardé, Laura Salavessa, Giulia Nigro, Stéphane Descorps-Declère, et al.. Shigella promotes major alteration of gut epithelial physiology and tissue invasion by shutting off host intracellular transport. Proceedings of the National Academy of Sciences of the United States of America , National Academy of Sciences, 2019, 10.1073/pnas.1902922116 . pasteur-02167942

**HAL Id: pasteur-02167942**

**<https://hal-pasteur.archives-ouvertes.fr/pasteur-02167942>**

Submitted on 3 Jun 2020

**HAL** is a multi-disciplinary open access archive for the deposit and dissemination of scientific research documents, whether they are published or not. The documents may come from teaching and research institutions in France or abroad, or from public or private research centers.

L'archive ouverte pluridisciplinaire **HAL**, est destinée au dépôt et à la diffusion de documents scientifiques de niveau recherche, publiés ou non, émanant des établissements d'enseignement et de recherche français ou étrangers, des laboratoires publics ou privés.

# *Shigella* promotes major alteration of gut epithelial physiology and tissue invasion by shutting off host intracellular transport

Mariana L. Ferrari<sup>1,2</sup>, Valérie Malardé<sup>1,2</sup>, Alexandre Grassart<sup>1,2</sup>, Laura Salavessa<sup>1,2,3</sup>, Giulia Nigro<sup>1,2</sup>, Stéphane Decorps-Declere<sup>4</sup>, John R. Rohde<sup>5</sup>, Pamela Schnupf<sup>6</sup>, Vanessa Masson<sup>7</sup>, Guillaume Arras<sup>7</sup>, Damarys Loew<sup>7</sup>, Philippe J. Sansonetti<sup>1,2,8\*</sup>, Nathalie Sauvonnet<sup>1,2\*</sup>

<sup>1</sup> Unité de Pathogénie Microbienne Moléculaire, Institut Pasteur, 28 rue du Dr Roux, 75015, Paris, France <sup>2</sup> U1202, INSERM, Paris, France <sup>3</sup> Université Paris Sud, Paris-Saclay University, Orsay, France <sup>4</sup> Institut Pasteur – Hub Bioinformatique et Biostatistique – C3BI, USR 3756 IP CNRS – 28 rue du Dr Roux, 75015, Paris, France <sup>5</sup> Department of Microbiology and Immunology, Dalhousie University, Halifax, NS, Canada <sup>6</sup> Institut Necker Enfants Malades, INSERM-CNRS, Laboratory of Host-Microbiota Interaction, 156 rue de Vaugirard, 75015 Paris, France <sup>7</sup> Institut Curie, PSL Research University, Centre de Recherche, Laboratoire de Spectrométrie de Masse Protéomique, 26 rue d'Ulm, Paris 75248 Cedex 05, France <sup>8</sup> Chaire de Microbiologie et Maladies Infectieuses, Collège de France, Paris, France

Submitted to Proceedings of the National Academy of Sciences of the United States of America

**Intracellular trafficking pathways in eukaryotic cells are essential to maintain organelle identity and structure, and to regulate cell communication with its environment. *Shigella flexneri* invades and subverts the human colonic epithelium by the injection of virulence factors through a type 3 secretion system (T3SS). In this work we report the multiple effects of two *S. flexneri* effectors, IpaJ and VirA, which target small GTPases of the Arf and Rab families, consequently inhibiting several intracellular trafficking pathways. IpaJ and VirA induce large-scale impairment of host protein secretion and block the recycling of surface receptors. Moreover, these two effectors decrease clathrin-dependent and -independent endocytosis. Therefore, *S. flexneri* infection induces a global blockage of host cell intracellular transport, affecting the exchange between cells and their external environment. The combined action of these effectors disorganizes the epithelial cell polarity, disturbs epithelial barrier integrity, promotes multiple invasion events and enhances the pathogen capacity to penetrate into the colonic tissue *in vivo*.**

bacteria | pathogen | secretion | endocytosis | polarity

## Introduction

Eukaryotic cells contain a complex array of intracellular membrane-bound compartments, which mediate cell communication with their environment by the bi-directional transport of proteins and lipids between the intracellular and extracellular spaces. This occurs via two main mechanisms: the secretory and the endocytic trafficking pathways. The efficient intracellular transport of molecules is regulated by GTPases of the Arf, Rab, Rho and dynamin families and is critical to maintain organelle identity and structure. Additionally, the coordination of intracellular trafficking with other pathways regulates vital processes including cell polarity, immunity, signaling and development as well as tissue and organ functions (1–3).

*Shigella* spp are Gram-negative intracellular bacteria causing bacillary dysentery or shigellosis (4). *Shigella* invades the colonic epithelium by using a type 3 secretion system (T3SS) that enables the injection of more than 20 virulence factors, the so-called effectors, into the cell (5, 6). These effectors then target multiple cellular functions to promote non-phagocytic uptake, followed by intracellular bacterial replication, cell-to-cell spreading, and subsequently leading to destruction of the colonic epithelium (7, 8). While the enzymatic functions for most effectors has been described and analyzed in cell culture, the mechanisms by which they cooperate with one another to promote infection remains largely unknown. *S. flexneri* induces Golgi apparatus fragmentation and reorganization of the endocytic compartment, leading to a block in secretion and receptor recycling (9). Among the

arsenal of injected effectors, two have been specifically implicated in targeting host cell small GTPases essential for Golgi-mediated secretory transport, namely: IpaJ and VirA. IpaJ is a cysteine protease catalyzing the cleavage of myristoylated glycine residues primarily from ADP-ribosylation factor (Arf) and Arf-like (Arl) proteins (10, 11). As a consequence, it was shown that IpaJ inhibits STING-mediated activation of the interferon (IFN) pathway by blocking STING translocation from the endoplasmic reticulum (ER) to ER-Golgi intermediate compartment (ERGIC) (12). Conversely, VirA was reported to impair host cell secretory transport, in addition to inhibiting autophagy (13, 14), by acting as a Rab-GTP activating protein (GAP) with preferential targeting of Rab1, as shown *in vitro* (13). Although the catalytic activities of these two effectors have been well described, it remains to be elucidated if both act in synergy or independently, and which changes they induce in the intestinal tissue during *S. flexneri* infection.

In eukaryotes, Arf and Rab protein families work together to regulate intracellular trafficking pathways. However, the exact mechanisms of coordination of action are not yet fully understood. Given that these small GTPases are targeted by both IpaJ

## Significance

***Shigella flexneri* is an enteroinvasive prokaryote that induces human bacillary dysentery. The delivery of around 30 bacterial effectors inside colonic epithelial cells allows the pathogen to invade, replicate and move into adjacent cells, hence subverting cellular and immune functions of its host. Intracellular trafficking pathways in eukaryotic cells are essential to regulate cell communication with their environment. Our work shows that two effectors of *Shigella flexneri* block three main trafficking pathways of its host cell: secretion, recycling and endocytosis, thereby freezing the exchange through the plasma membrane. As a consequence, *Shigella flexneri* disorganizes the epithelial cell polarity, disturbs epithelial barrier integrity, and enhances the pathogen capacity to penetrate into the colonic tissue *in vivo*.**

## Reserved for Publication Footnotes

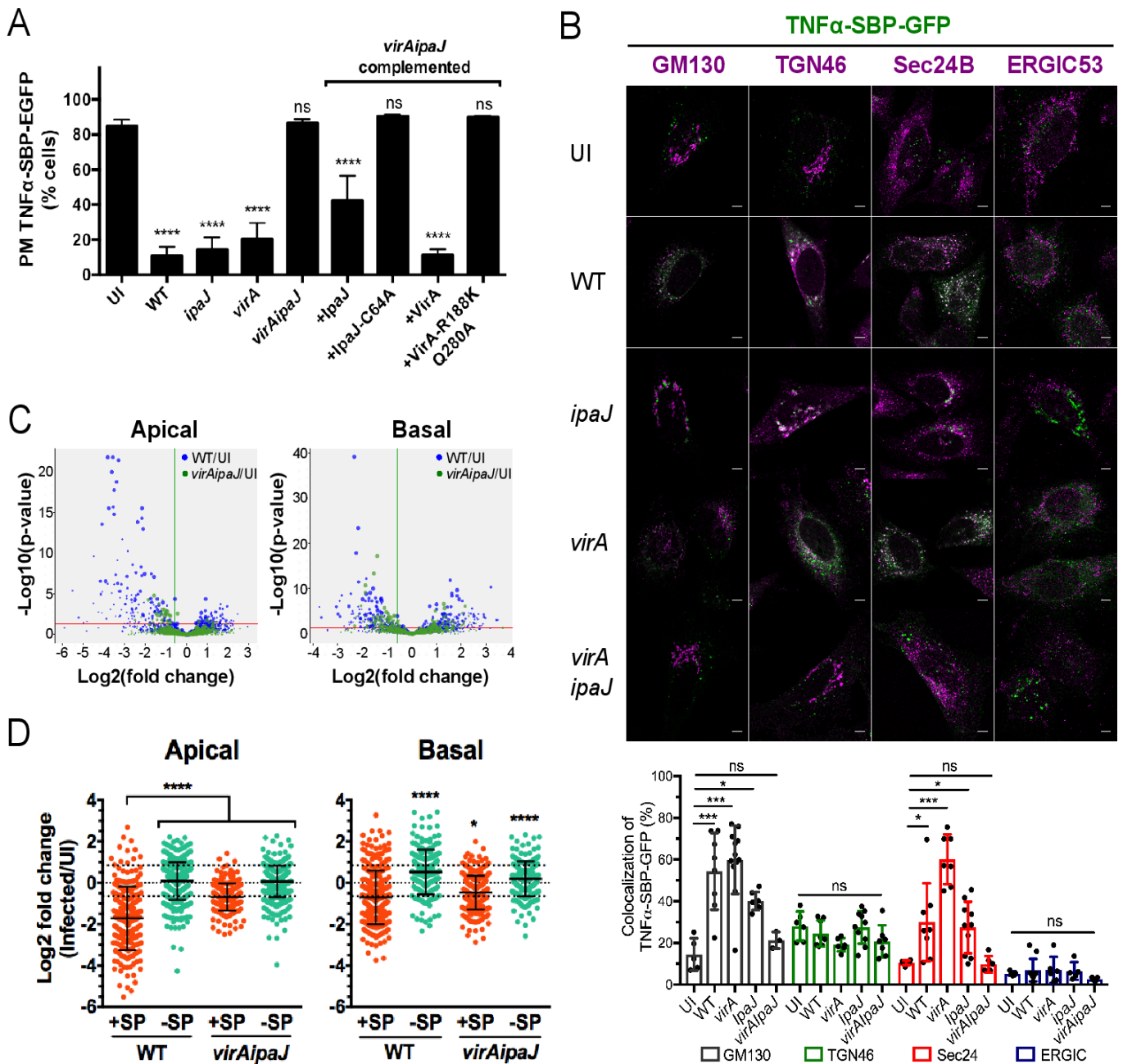


**Fig. 1. *S. flexneri* effectors *IpaJ* and *VirA* have a global effect on conventional secretion.** (A) *IpaJ* and *VirA* effectors block the anterograde transport of the cytokine TNF $\alpha$ . HeLa cells stably expressing the RUSH cargo TNF $\alpha$ -SBP-GFP and the molecular hook Streptavidin-KDEL were uninfected (UI) or infected for 1 hour with WT-dsRed or the dsRed-expressing mutants *ipaJ*, *virA*, *virAipaJ*, or with *virAipaJ* complemented with *plpA*-myc, *plpA*-C64-myc, *pVirA*-myc, or *pVirA*-R188K/Q280A-myc. Cells were then incubated with biotin for 1 hour, fixed and surface-stained for TNF $\alpha$ -SBP-GFP with anti-GFP DyLight 680 conjugated antibody. The arrival of TNF $\alpha$ -SBP-GFP to the plasma membrane (PM) was monitored by flow cytometry. Mean SD.  $n = 3$ . \*\*\*\* $p < 0.0001$ , ns: non-significant (one-way ANOVA, Dunnett's *post-hoc* test, compared to UI). (B) TNF $\alpha$ -SBP-GFP is retained in different subcellular compartments upon *S. flexneri* infection. HeLa cells stably expressing the RUSH cargo TNF $\alpha$ -SBP-GFP and the molecular hook Streptavidin-KDEL were uninfected (UI) or infected for 1 hour and incubated with biotin for 1 additional hour. Cells were fixed, permeabilized and stained with various subcellular markers: anti-GM130 (*cis*-Golgi), anti-ERGIC53 (ERGIC), anti-Sec24B (ERES), anti-TGN46 (*trans*-Golgi network). Scale bar: 5  $\mu$ m. Levels of colocalization between TNF $\alpha$ -SBP-GFP and the different sub-cellular markers were quantified by SODA plugin in ICY software. Mean SD,  $5 < n < 12$  cells. \* $p < 0.05$ ; \*\*\* $p < 0.001$  (one-way ANOVA, Dunnett's *post-hoc* test). (C-D) *S. flexneri* blocks globally the host conventional secretion. Caco-2/TC7 cells were labeled with SILAC amino acids, grown in transwell filters and infected with WT *S. flexneri* or the mutant *virAipaJ*. After 4.5 hours, the apical and basal media were collected and analyzed by mass spectrometry to determine the relative abundance of secreted proteins in the infected, in comparison with UI conditions. (C) Volcano plots displaying log<sub>2</sub> fold-changes of secreted proteins from WT or *virAipaJ* infected cells in comparison with UI conditions in apical and basal media. (D) Dot plots represent log<sub>2</sub> of infected/UI ratio for proteins with (red) and without (green) signal peptide (SP). Mean SD. 217 >  $n$  > 394 proteins for Apical secretome; 194 >  $n$  > 281 proteins for Basal secretome. \* $p < 0.05$ , \*\*\*\* $p < 0.0001$  (one-way ANOVA, Dunnett's *post-hoc* test, each condition compared to Apical or Basal secreted proteins containing signal peptide (+SP)).

and *VirA*, it raises the question if these effectors further affect

other trafficking pathways in addition to the known secretory transport.

273  
274  
275  
276  
277  
278  
279  
280  
281  
282  
283  
284  
285  
286  
287  
288  
289  
290  
291  
292  
293  
294  
295  
296  
297  
298  
299  
300  
301  
302  
303  
304  
305  
306  
307  
308  
309  
310  
311  
312  
313  
314  
315  
316  
317  
318  
319  
320  
321  
322  
323  
324  
325  
326  
327  
328  
329  
330  
331  
332  
333  
334  
335  
336  
337  
338  
339  
340

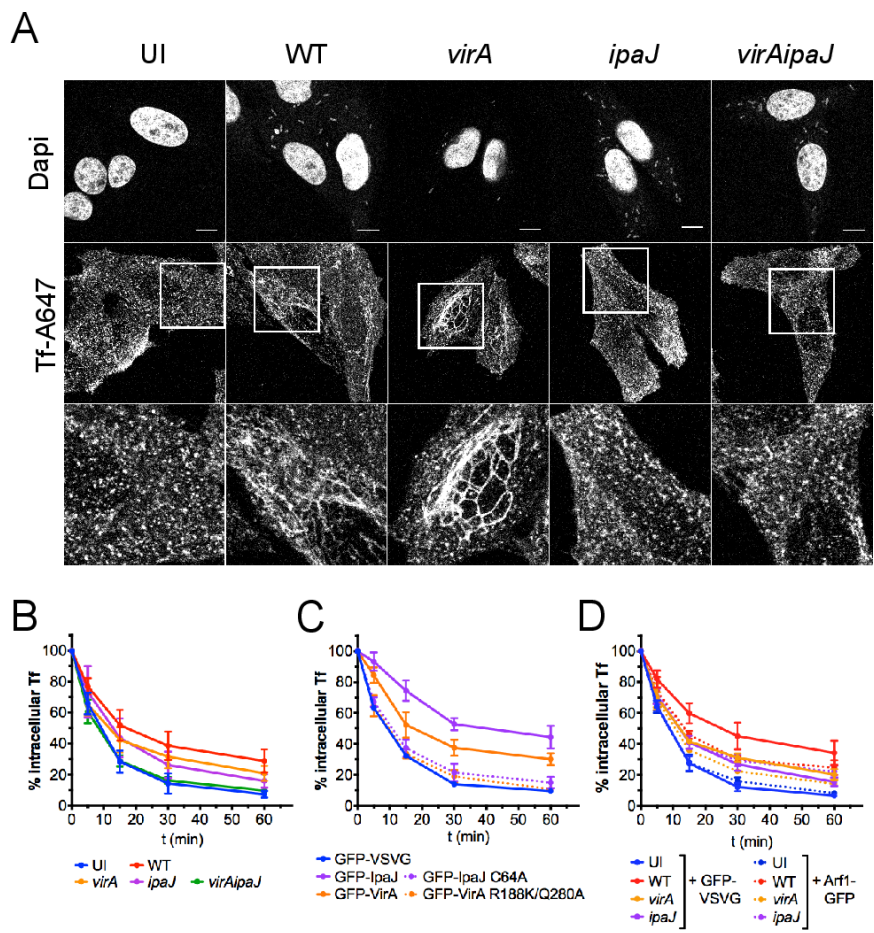


**Fig. 2. Both *S. flexneri* IpaJ and VirA affect TfR recycling.** (A) IpaJ induces endosomal tubulation. Hep2 cells loaded with Tf-AF647 were uninfected (UI) or infected for 1 hour with WT, *virA*, *ipaJ* or *virAipaJ* strains, fixed and stained with Dapi (nuclei and bacteria). Scale bar: 10  $\mu$ m. (B-D) Tf recycling kinetics monitored by FC. Hep2 cells non-transfected or transfected with the indicated plasmids were loaded with Tf-AF647 and were left UI or infected for 1 hour with the indicated *S. flexneri* strains. Cells were then chased with unlabeled holo-Tf, and the loss of intracellular Tf-AF647 fluorescence was monitored over time. (B) IpaJ and VirA block Tf recycling. Cells were UI or infected with WT, *virA*, *ipaJ* or *virAipaJ* strains followed by Tf recycling kinetic. (C) Tf recycling is inhibited by IpaJ and VirA catalytic activities. Cells were transfected with GFP-VSVG (control), GFP-VirA, GFP-IpaJ or their mutated versions GFP-VirA-R188K/Q280A and GFP-IpaJ-C64A. Tf recycling kinetic was performed 24 hours post-transfection. (D) Arf1-GFP overexpression partially recovers Tf recycling. Cells were transfected either with GFP-VSVG (control) or Arf1-GFP, loaded with Tf-AF647, UI or infected with WT, *virA* or *ipaJ* strains followed by Tf recycling. Means SD from at least 3 independent experiments are shown (statistical tests in Fig. S2D-F).

Here, we demonstrate that these two effectors independently block global host cell secretion and concurrently operate to impair receptor recycling. Moreover, we report that IpaJ and VirA decrease receptor-mediated endocytosis. Our results illustrate how *S. flexneri* “freezes” the invaded host cell by globally interfering on multiple intracellular transport systems, thereby affecting the exchange of molecules between cells and their environment and consequently cell and tissue functions.

**Results**

***S. flexneri* effectors IpaJ and VirA globally impair conventional secretion**

Both IpaJ and VirA *S. flexneri* effectors have been shown to affect Golgi-mediated transport in host cells (10, 13), raising the question as to whether these effectors operate in synergy or independently. To address this, we first quantified the secretion level of the cytokine TNF $\alpha$  upon infection with wild type (WT) *S. flexneri*, or the mutant strains *ipaJ*, *virA*, or *virAipaJ*. We used the RUSH system (15) to follow the synchronized trafficking of the reporter TNF $\alpha$ -SBP-GFP from the endoplasmic reticulum to the plasma membrane of epithelial cells (Fig. 1A). Infection with WT *S. flexneri* blocked 75% of the anterograde trafficking of TNF $\alpha$ -SBP-GFP when compared to uninfected cells (UI), in line with previous reports on other cargoes (9, 13). Similar results were obtained when cells were infected with either *ipaJ* or *virA* *S. flexneri* single mutants. However, in cells infected by the *virAipaJ* double mutant, TNF $\alpha$ -SBP-GFP transport levels were similar to the uninfected condition (Fig. 1A). This differential effect of trafficking during infection by WT, *ipaJ*, *virA* and *virAipaJ* was not due to impairment in bacterial invasion by the mutant strains (Fig.

S1A). Complementation of the double mutant with either pVirA-myc or pIpaJ-myc was sufficient to restore, at least partially, the secretion inhibitory phenotype obtained with WT bacteria. As expected, complementation with the mutated versions of these effectors in their catalytic sites, pVirA-R188K/Q280A-myc or pIpaJ-C64A-myc (10, 13), did not affect the normal trafficking of TNF $\alpha$ -SBP-GFP (Fig. 1A). Altogether, these results show that each effector, IpaJ and VirA, is sufficient to block anterograde transport of the cargo via their catalytic activities and hence acts largely independently.

To determine in which subcellular compartment TNF $\alpha$ -SBP-GFP was retained upon *S. flexneri* infection, we utilized immunostaining of various subcellular compartments after 1 hour of synchronized trafficking and quantified the percentage of colocalization using a statistical object-based method (Fig. 1B). In uninfected and *virAipaJ* infected cells, TNF $\alpha$ -SBP-GFP was mostly at plasma membrane (Fig. 1A), but the minor intracellular pool was mostly colocalized with *trans*-Golgi network (TGN) labeled with TGN46 (21-28%) and with *cis*-Golgi remnants (GM130-positive compartment, 14-20%) (Fig. 1B). By contrast, in WT-infected cells TNF $\alpha$ -SBP-GFP was mostly intracellular (Fig. 1A) and colocalized with GM130 (54%), Sec24B (29%), a marker of ER exit sites (ERES), and with TGN46 (24%). This reveals that *S. flexneri* WT infection blocked the Golgi-mediated transport at different stages, mainly at ERES and at *cis*-Golgi. Interestingly, infection with *virA* or *ipaJ* mutants resulted in a phenotype similar to the WT strain except that in absence of IpaJ, TNF $\alpha$ -SBP-GFP was strongly colocalized with Sec24 (60%, Fig. 1B). These data suggest that the retention in the Sec24B-positive compartment was due to the action of IpaJ. We could not observe colocalization

341  
342  
343  
344  
345  
346  
347  
348  
349  
350  
351  
352  
353  
354  
355  
356  
357  
358  
359  
360  
361  
362  
363  
364  
365  
366  
367  
368  
369  
370  
371  
372  
373  
374  
375  
376  
377  
378  
379  
380  
381  
382  
383  
384  
385  
386  
387  
388  
389  
390  
391  
392  
393  
394  
395  
396  
397  
398  
399  
400  
401  
402  
403  
404  
405  
406  
407  
408

409  
410  
411  
412  
413  
414  
415  
416  
417  
418  
419  
420  
421  
422  
423  
424  
425  
426  
427  
428  
429  
430  
431  
432  
433  
434  
435  
436  
437  
438  
439  
440  
441  
442  
443  
444  
445  
446  
447  
448  
449  
450  
451  
452  
453  
454  
455  
456  
457  
458  
459  
460  
461  
462  
463  
464  
465  
466  
467  
468  
469  
470  
471  
472  
473  
474  
475  
476

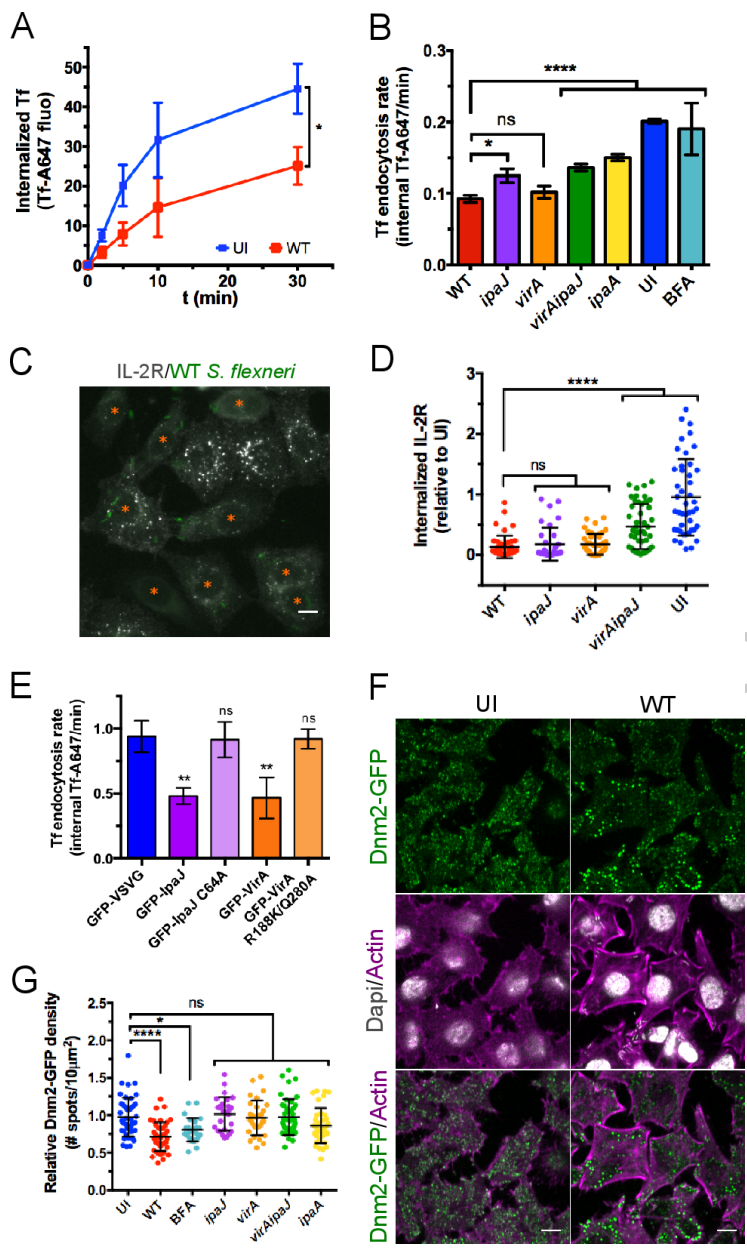


**Fig. 3. *S. flexneri* affects clathrin-dependent and independent endocytosis.** (A) Tf uptake is decreased upon WT-infection. Hep2 cells were left uninfected (UI) or infected with the WT strain for 30 min and then incubated for different time-points with Tf-AF647 at 37 °C. After an acidic wash, the total internal Tf-AF647 fluorescence was quantified by FC. Mean SD, n = 4. \*p<0.05 (unpaired two-tailed Welch's t-test performed on AUC). (B) Different *S. flexneri* effectors decrease the Tf endocytosis rate. Hep2 cells were left UI or infected with GFP-expressing WT or mutant strains for 90 min, prior to monitor by FC the Tf-AF647 uptake over time. Mean SD. n 3. (C-D) IL-2R endocytosis is decreased upon WT *S. flexneri* infection. (C) UI or WT-infected Hep2β cells were incubated with an anti-IL-2Rβ-Cy3 antibody for 15 min at 37°C, fixed and subjected to fluorescent microscopy. Scale bar: 10 μm. (D) Quantification of IL-2R endocytosis. Cells either UI or infected by WT, *ipaJ*, *virA* and *virAipaJ* *S. flexneri* strains for 90 min were incubated with an anti-IL-2Rβ-Cy3 antibody for 30 min at 37°C, fixed, subjected to confocal fluorescence microscopy and analyzed by quantifying the fluorescence intensity of IL-2R-positive vesicles per cell. Mean SD. 35<n<48 cells. (E) Tf endocytosis kinetic was performed 24 hours post-transfection. Mean SD. n = 3. (F-G) *S. flexneri* decrease Dnm2-GFP density at plasma membrane. Hep2β Dnm2-GFP cells were UI, treated with BFA for 30 min or infected with WT or mutant strains for 90 min. Cells were fixed and labeled with rabbit anti-LPS followed by anti-rabbit-A405 and Phalloidin-A647 prior to confocal (F) or TIRF (G) imaging. Scale bar: 10 μm. (G) Quantification of Dnm2-GFP density (number of Dnm2-GFP spots/area) at plasma membrane from TIRF microscopy images. Mean SD. 27<n<45 cells pooled from 2 independent experiments. B-D-E-G, one-way ANOVA, Dunnett's *post-hoc* test. ns: non significant; \*p<0.05; \*\*p<0.01; \*\*\*\*p<0.0001.

of TNFα-SBP-GFP with ERGIC53, a marker of the ERGIC, in any of the conditions tested (Fig. 1B). Taken together, our data show that IpaJ and VirA block the anterograde trafficking at multiple stages, confirming their independent action in blocking host cell secretion.

To investigate the global effects of *S. flexneri* infection on the secretory transport in a polarized cell system, we used the SILAC technology coupled to LC-MS/MS (16). Polarized Caco-2/TC7 cells labeled with “medium” amino acids were uninfected, and cells labeled with “heavy” amino acids were infected with either WT *S. flexneri* or the mutant *virAipaJ*. After 5 hours of infection, the SILAC-labeled secretome-containing supernatants from the apical and basal side were collected and treated for mass spectrometry analysis in order to determine the relative abundance of peptides between infected and uninfected samples (Fig. S1B). Fold change-based GO enrichment analysis showed that apical and basal secretome proteins were more than 4-times enriched in extracellular proteins in comparison to the human

theoretical proteome, hence revealing the good quality of our analysis. We quantified 148 proteins in the apical and 136 in the basal supernatants that were differentially secreted in WT *S. flexneri* infected cells when compared to uninfected cells (UI), from which 125 (84%) and 79 (58%) proteins, respectively, were less secreted (Fig. 1C, Table S1). This secretion impairment was independent of global changes in the proteome of infected cells (Fig. S1C). In addition, tight junctions and cell viability were not affected during the secretome collection (Fig. S1D-F). Among the differentially secreted proteins, 116 (92.8%) of the apical and 64 (81%) of the basal proteins contained predicted cleavable signal peptides indicating targets of the conventional secretory pathway (Fig. 1D). In contrast, analysis of the same proteins from the *virAipaJ*-infected samples revealed only a marginal impairment on the secretion of signal-peptide containing proteins; indeed, the mean fold-change was less striking than for the WT-infected secretomes (Fig. 1D, Table S1). Taken together, these results indicate that *S. flexneri* infection affects the conventional

477  
478  
479  
480  
481  
482  
483  
484  
485  
486  
487  
488  
489  
490  
491  
492  
493  
494  
495  
496  
497  
498  
499  
500  
501  
502  
503  
504  
505  
506  
507  
508  
509  
510  
511  
512  
513  
514  
515  
516  
517  
518  
519  
520  
521  
522  
523  
524  
525  
526  
527  
528  
529  
530  
531  
532  
533  
534  
535  
536  
537  
538  
539  
540  
541  
542  
543  
544

545  
546  
547  
548  
549  
550  
551  
552  
553  
554  
555  
556  
557  
558  
559  
560  
561  
562  
563  
564  
565  
566  
567  
568  
569  
570  
571  
572  
573  
574  
575  
576  
577  
578  
579  
580  
581  
582  
583  
584  
585  
586  
587  
588  
589  
590  
591  
592  
593  
594  
595  
596  
597  
598  
599  
600  
601  
602  
603  
604  
605  
606  
607  
608  
609  
610  
611  
612

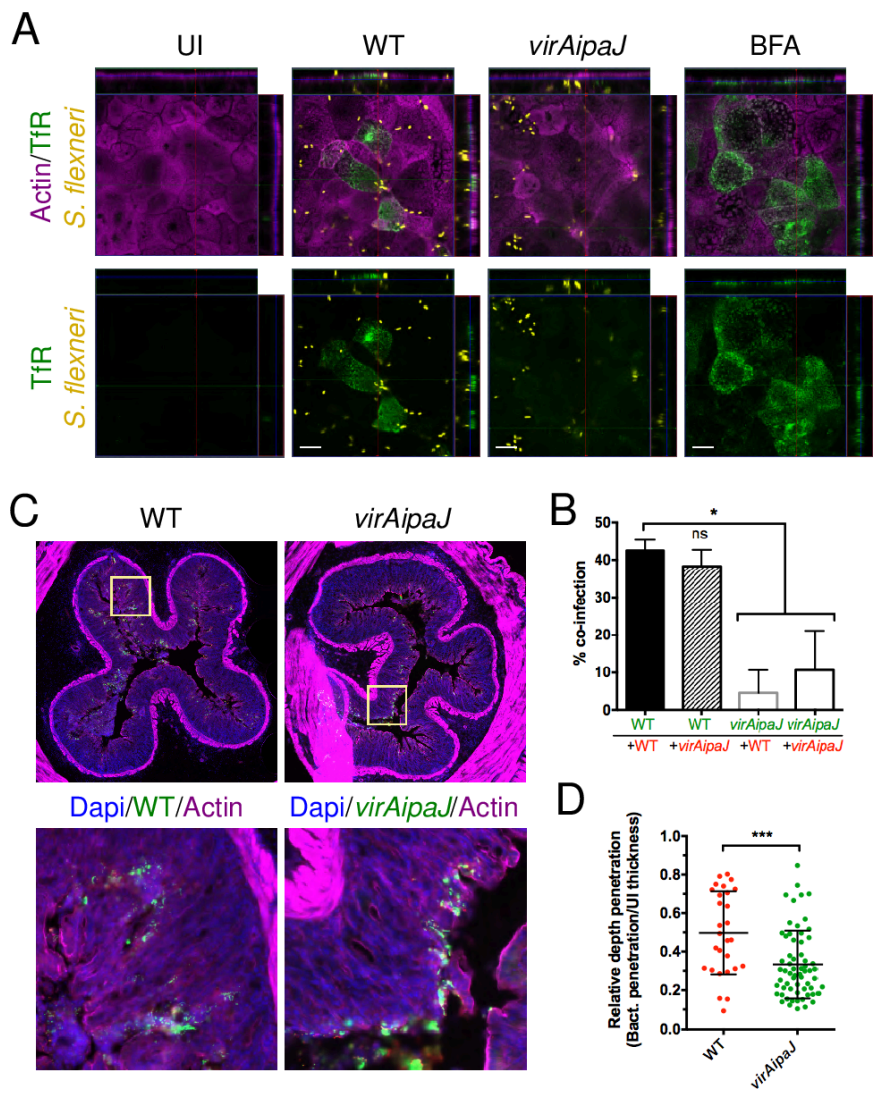


**Fig. 4. *S. flexneri* invasion disrupts cell polarity and colonic epithelium**(A) *S. flexneri* delocalizes the Tfr to the apical domain of polarized Caco-2/TC7 cells. Cells were left uninfected (UI), infected with the WT or *virAipaJ* strains for 5h or treated with BFA for 30 min, prior to fixation without permeabilization and subsequent apical surface staining with an anti-Tfr (OKT9) recognizing the extracellular domain of the receptor. Scale bars: 10  $\mu$ m. (B) IpaJ and VirA enhance re-infection of polarized cells. Caco-2/TC7 cells were primo-infected with GFP-expressing WT or *virAipaJ* strains (green) for 4 hours, and then re-infected with the same strains expressing dsRed for 2 more hours (red). The % of co-infection was quantified by determining the % of primo-infected cells (GFP positive) that were re-infected with dsRed-expressing bacteria. Mean SD, n = 4. ns: non significant; \* p<0.05 (Kruskal-Wallis test followed by Dunn's *post-hoc* test). (C-D) *S. flexneri* WT has a deeper penetration than *virAipaJ* mutant into the Guinea pig colonic tissue. (C) Colonic tissue from animals infected with GFP-expressing WT or *virAipaJ* mutant, 8 hours post-infection, were stained with Phalloidin-A647 (actin) and Dapi (nuclei). (D) The relative depth penetration of both strains into the colonic tissue was measured by their penetration from the epithelial surface compared to the total epithelial mucosa thickness at 4 hours post-infection. Mean SD. 28<n<48 focus of infection pooled from 2 biological replicates. \*\*\*p<0.001 (Mann-Whitney test).

secretory pathway in a global manner, and that this is mediated by the action of both IpaJ and VirA effectors.

Among the proteins less secreted by WT-infected cells, the most represented class were hydrolytic enzymes, like proteases (cathepsin D, carboxypeptidase M) and enzyme regulators. However, we also found cell receptors (LDLR, HGFR), lipid transporters (apolipoproteins), proteins related to cell adhesion and extracellular matrix (ECM) (laminins), and immunomodulators (IL6ST) (Table S1). The secretion inhibition of this wide array of proteins may have severe consequences on cell polarity and intestinal tissue organization and functions.

***S. flexneri* effectors IpaJ and VirA both block the host cell recycling pathway**

As IpaJ and VirA effectors are targeting small GTPases from the Arf and Rab families, which are important for normal endosomal functioning (1, 3), we further investigated if they were also implicated in the previously described reorganization of the endosomal compartment and impairment of transferrin (Tf) receptor (TfR) recycling (9). We loaded Hep2 cells with fluorescent Tf coupled to Alexa Fluor 647 (Tf-AF647), prior to infection with WT, *virA*, *ipaJ* or *virAipaJ* strains (Fig. 2A). In line with what was previously reported (9), after 1 hour of infection with WT *S. flexneri* we observed an extensive formation of membrane tubules labeled with Tf-AF647, which resembled

the phenotype induced by the drug brefeldin A (BFA) (Fig. S2A) (17). A comparable, tubular phenotype was observed when cells were infected with the *virA* mutant strain. In contrast, in cells infected with either the *ipaJ* or *virAipaJ* mutant, Tf-AF647 was located in punctate vesicles throughout the cytoplasm, resembling the uninfected control (Fig. 2A). These findings demonstrate that IpaJ is involved in endosomal compartment tubulation. As shown in the case of BFA-treated cells (17, 18) (Fig. S2B), the formation of endosomal tubules is not necessarily linked to a striking recycling impairment. We therefore assessed TfR recycling kinetics by pulse-chase experiments. Here, cells were loaded with Tf-AF647, uninfected or infected for 1 hour with the GFP-expressing WT or mutant *S. flexneri* strains, and then chased with the unlabeled holo-Tf for different time-points prior to analysis by flow cytometry (FC) (Figs. 2B, S2D). We observed a notable reduction of Tf-AF647 recycling in WT-infected cells, whereby 50% of the internalized Tf-AF647 recycled back to the plasma membrane in 17 minutes, as compared to only 9 minutes for uninfected cells. In addition to the observed time delay induced by the WT strain, Tf recycling was also blocked, as indicated by 29% retention of Tf-AF647 at the 60 minutes kinetic end-point. When cells were infected with the *ipaJ* or *virA* mutant, an intermediate phenotype was observed while the *virAipaJ* double mutant had normal levels of Tf recycling similarly to uninfected conditions (Figs. 2B, S2D).

613  
614  
615  
616  
617  
618  
619  
620  
621  
622  
623  
624  
625  
626  
627  
628  
629  
630  
631  
632  
633  
634  
635  
636  
637  
638  
639  
640  
641  
642  
643  
644  
645  
646  
647  
648  
649  
650  
651  
652  
653  
654  
655  
656  
657  
658  
659  
660  
661  
662  
663  
664  
665  
666  
667  
668  
669  
670  
671  
672  
673  
674  
675  
676  
677  
678  
679  
680

681 These results demonstrate that a combined action of these two  
682 effectors is required to efficiently block receptor recycling in the  
683 host cell. Further, we confirmed that the inhibitory effect of IpaJ  
684 and VirA on receptor recycling is due to their catalytic activities.  
685 While their ectopic expression in Hep2 cells dramatically decreased  
686 the Tf recycling rate (Figs. 2C, S2E), control levels of Tf  
687 recycling were obtained when the VirA-R188K/Q280A or IpaJ-  
688 C64A mutated versions were expressed (Figs. 2C, S2E). To gain  
689 further insights into the mechanisms at play, we overexpressed  
690 one of the targets of IpaJ, the small GTPase Arf1 fused to GFP,  
691 prior to infection with dsRed-expressing bacterial strains (Figs.  
692 2D, S2F). In uninfected cells the Tf recycling rate remained  
693 unchanged despite overexpression of either Arf1-GFP or GFP-  
694 VSFG, which served as a transfection control (Figs. 2D, S2C-F).  
695 Interestingly, the rate of Tf recycling was faster in cells infected  
696 by the IpaJ-expressing strains, WT and *virA*, and overexpressing  
697 Arf1-GFP (Figs. 2D, S2F). In contrast, in *ipaJ*-infected cells,  
698 the recycling kinetics remained unchanged by Arf1 overexpression.  
699 These results strongly suggest that IpaJ slows down Tf recycling  
700 by targeting Arf1. Overall, we demonstrate that the two *S. flexneri*  
701 effectors, IpaJ and VirA, present catalytic activities that together  
702 strongly inhibit two major trafficking pathways, secretion and  
703 recycling, that are implicated in the delivery of molecules to the  
704 cellular surface.

### 705 *S. flexneri* infection affects different host endocytic pathways

706 Next, we investigated whether *S. flexneri* directly blocked the  
707 endocytic pathways. In the first instance, we aimed to test *S.*  
708 *flexneri* infection on clathrin-dependent endocytosis (CDE). To  
709 do this, we performed Tf uptake experiments using Tf, a *bona fide*  
710 cargo of CDE (19). Hep2 cells were either left uninfected or were  
711 infected for 90 min with GFP-WT *S. flexneri*, prior to incubation  
712 with Tf-AF647 at 37°C for different time-points, and followed by  
713 FC analysis. In WT-infected cells, we observed a 54% reduction  
714 in the endocytosis rate, as well as a significant inhibition of the  
715 total Tf uptake at the 30 minutes end-point (Fig. 3A-B), which  
716 was independent of the surface expression of TfR (Fig. S3A). This  
717 defect on Tf uptake was also observed in WT-infected polarized  
718 Caco-2/TC7 cells, after basolateral incubation with fluorescent Tf  
719 (Figs. S3C-D). In order to test if other endocytic pathways were  
720 affected by *S. flexneri* infection, we assayed for IL-2 receptor (IL-  
721 2R) uptake, a well-described marker of a clathrin-independent  
722 endocytosis (CIE) pathway (20). Hep2 $\beta$  cells, stably expressing the  
723 IL-2R $\beta$  chain, were left uninfected or infected with WT *S.*  
724 *flexneri* strain for 90 min and then incubated with an anti-IL-2R $\beta$   
725 chain antibody coupled to Cy3 for 15 min, fixed and analyzed by  
726 fluorescent microscopy (21) (Fig. 3C). We observed a dramatic  
727 reduction in IL-2R $\beta$  uptake in WT-infected cells after 15 min  
728 of endocytosis when compared to uninfected cells (Fig. 3D).  
729 These results indicate that WT *S. flexneri* reduces both clathrin-  
730 dependent and -independent endocytosis pathways.

731 As IpaJ and VirA effectors target key players in regulating  
732 intracellular transport, we asked whether they had an impact  
733 on this inhibition of endocytosis. Thus, we infected cells with *S.*  
734 *flexneri* WT, *virA*, *ipaJ* and *virAipaJ* strains and performed Tf-  
735 AF647 uptake kinetics. We observed a partial recovery of Tf  
736 uptake when infecting cells with the three mutant strains (Fig.  
737 3B), indicating that both IpaJ and VirA decrease endocytosis.  
738 This IpaJ/VirA-dependent Tf endocytosis inhibition is stronger  
739 than BFA, which does not induce significant changes in contrast to  
740 uninfected conditions (Fig. 3B), as previously reported (17, 22).  
741 In addition, we confirmed that the inhibitory effect of IpaJ and  
742 VirA on endocytosis was due to their catalytic activities, as their  
743 ectopic expression in Hep2 cells considerably decreased Tf uptake  
744 but not when their catalytic-inactive forms were expressed (Fig. 3E).  
745 In order to determine whether other effectors were involved in  
746 the Tf uptake impairment, we next tested a panel of *S. flexneri*  
747 mutants lacking effectors with different cellular targets (Figs. 3B,

749 S3B). Interestingly, we also found a partial recovery of Tf uptake  
750 in cells infected with the *ipaA* mutant, which lacks the vinculin-  
751 binding protein IpaA (Fig. 3B) (23). Again, the differences in  
752 Tf uptake rate between mutant strains and WT could not be  
753 explained by differences of TfR surface expression (Fig. S3A).  
754 Overall, these results demonstrate that three *S. flexneri* effectors,  
755 IpaJ, VirA and IpaA, inhibit endocytosis in the host cell.

756 To gain more insight into the mechanisms by which *S. flexneri*  
757 affects CDE and CIE, we looked at dynamin 2 (Dnm2), an  
758 enzyme implicated in both pathways and involved in the pinching-  
759 off of vesicles from the plasma membrane (24). To this end, we left  
760 uninfected or infected Hep2 $\beta$  Dnm2-GFP genome-edited cells  
761 (25) with WT *S. flexneri* and analyzed the Dnm2-GFP distribution  
762 at plasma membrane by total internal reflection fluorescence  
763 (TIRF) microscopy (Fig. 3F-G). Upon WT-infection, we observed  
764 a 27% reduction of Dnm2-GFP at the plasma membrane (Fig.  
765 3F), which was quantified by image analysis (Fig. 3G). This  
766 reduction was not due to a decrease of total Dnm2-GFP levels (Fig.  
767 S3E), but likely linked to a reduced recruitment of Dnm2-GFP  
768 to the plasma membrane and hence to endocytic sites. Similar  
769 results were obtained when we analyzed the clathrin light chain  
770 A (CLC) behavior in Hep2 $\beta$  CLC-GFP genome-edited cells (25)  
771 (Fig. S3F-G). Interestingly, this phenotype was correlated with  
772 IpaJ and VirA expression since cells infected with either the single  
773 or the double *virAipaJ* mutants recovered the normal Dnm2-GFP  
774 and CLC-GFP recruitment at the plasma membrane (Figs. 3G,  
775 S3G). In addition, BFA-treated cells also showed a reduction in  
776 Dnm2-GFP at the plasma membrane, although smaller than upon  
777 infection with WT bacteria (Fig. 3G). In contrast, IpaA led to  
778 a marginal effect on Dnm2-GFP distribution (Fig. 3G). These  
779 results indicate that Dnm2, a key host factor involved in both  
780 CDE and CIE, is affected by *S. flexneri*, explaining the observed  
781 reduction in the uptake of both Tf and IL-2R upon infection.  
782 Altogether, our results show how IpaJ and VirA effectors induce  
783 multifactorial defects on the general intracellular trafficking of  
784 host cells.

### 785 IpaJ and VirA disorganize cell polarity and colonic tissue 786 structure

787 According to our results, IpaJ and VirA are responsible for  
788 blocking three intracellular trafficking pathways: secretion, recycling  
789 and endocytosis. We therefore asked whether this vesicular  
790 trafficking blockage affected the maintenance of cell polarity.  
791 Therefore, we infected polarized Caco-2/TC7 cells and stained the  
792 surface TfR, which is usually expressed in the basolateral  
793 domain of polarized cells. We observed a pool of the TfR  
794 localizing at the apical cell domain upon WT *S. flexneri* infection,  
795 similarly to what has been previously reported in BFA-treated  
796 cells (26) (Fig. 4A). On the contrary, the TfR did not localize at  
797 the apical domain of uninfected or *virAipaJ*-infected cells (Fig.  
798 4A). These results indicate that IpaJ and VirA lead to a loss in  
799 the polarized transport of TfR, hence highlighting the *S. flexneri*-  
800 mediated disorganization of epithelial polarity.

801 We next asked whether these two effectors, by disrupting cell  
802 polarity and epithelial barrier integrity, promoted new invasion  
803 events in a second round of bacterial infection (Figs. 4B, S4A).  
804 For that, we first infected cells with either GFP-expressing WT  
805 or *virAipaJ* strains, and then with the same strains but expressing  
806 dsRed. We then quantified the percentage of cells co-infected by  
807 the GFP and dsRed strains (Figs. 4B, S4A). We observed that  
808 cells primo-infected with the WT strain were more prone to be re-  
809 infected with either the WT or the *virAipaJ* strain when comparing  
810 with *virAipaJ* primo-infected cells, which were poorly re-infected  
811 (Fig. 4B). This result indicates that IpaJ and VirA favor multiple  
812 invasion events, thereby enhancing the efficiency of infection.

813 Next, we used an *in vivo* model of infection to analyze whether  
814 the trafficking impairment caused by IpaJ and VirA induced  
815 changes in the colonic epithelial structure and function. We in-  
816

817 fected Guinea pigs intrarectally (27, 28) with *S. flexneri* WT or  
818 the double mutant *virAipaJ*. First, we observed a compact Golgi  
819 structure in colonocytes from *virAipaJ*-infected animals as com-  
820 pared to a fragmented Golgi apparatus observed in WT infected  
821 animals, confirming the combined action of IpaJ and VirA on  
822 disrupting Golgi structure *in vivo* (Fig. S4B). We then analyzed  
823 the relative depth penetration of WT and *virAipaJ* strains from  
824 the epithelial surface within the colonic tissue (Figs. 4C-D, S4B).  
825 We observed and quantified a 40% decrease in the penetration  
826 depth of the *virAipaJ* mutant in contrast to the WT strain. This  
827 difference cannot be explained by a spreading defect in the  
828 *virAipaJ* mutant, as the plaques formed on a cell monolayer by the  
829 *virAipaJ* mutant after 48 hours of infection are only 3% smaller  
830 than the ones formed by the WT strain (Fig. S4C). Overall,  
831 these results indicate that IpaJ and VirA, by the induction of a  
832 general trafficking impairment, are critical for intestinal epithelial  
833 invasion *in vivo*.

## 834 Discussion

835 In this study, we showed how two *S. flexneri* effectors, IpaJ and  
836 VirA, are necessary and sufficient to block several key intracellu-  
837 lar trafficking pathways in invaded cells, inducing a “frozen” state  
838 in which cells are no longer able to exchange molecules with their  
839 environment. These results were observed *in vitro* both in non-  
840 polarized and polarized cells. Moreover, we were able to show *in*  
841 *in vivo* the impact of some of the functions of these effectors on the  
842 efficient intestinal invasion by the bacteria.

843 Our work confirmed, in the context of cellular *S. flexneri* infec-  
844 tion, the secretion blockage described when overexpressing either  
845 of the effectors, IpaJ or VirA (10, 13). This is not trivial as EspG  
846 for instance, the enterohaemorrhagic and enteropathogenic *Es-*  
847 *cherichia coli* (EHEC/EPEC) homolog of *Shigella* VirA, does not  
848 affect the secretory transport during EHEC infection (29), but  
849 only during ectopic overexpression. This suggests that Rab1 is  
850 not targeted *in vivo* by EHEC EspG, and illustrates how the  
851 overexpression of certain virulence factors might induce pheno-  
852 types that are not observed during natural infection. However,  
853 the fact that VirA blocks the secretory transport in *S. flexneri*-  
854 infected cells strongly suggests that Rab1 is a VirA substrate,  
855 but does not exclude the possibility that other Rabs might be  
856 targeted by this effector. In line with this, we demonstrated that  
857 VirA, in combination with IpaJ, impairs the normal recycling  
858 of cell receptors. VirA, in contrast to EPEC/EHEC EspG, was  
859 shown *in vitro* to have a broader range of specificity towards Rab  
860 GTPases (13). This strongly suggests that endosomal Rabs, such  
861 as Rab11, Rab35 or Rab22 (30), are targeted and inactivated by  
862 VirA, explaining part of the recycling impairment. Interestingly,  
863 it was reported that EspG reduces surface receptor levels and  
864 receptor recycling in EHEC infected cells (29) and this is due to  
865 the modulation of an Arf6:Rab35 signaling axis (31). Moreover,  
866 EspG was shown to interact with Arf GTPases and PAK (13, 32).  
867 However, unlike in EHEC infection, a scaffolding role of VirA  
868 modulating Rab-Arf signaling has not been described so far for *S.*  
869 *flexneri*. On the other hand, our results show that IpaJ and VirA  
870 work in concert to induce an additive defect in receptor recycling.  
871 Although IpaJ activity slows down Tf recycling by targeting Arf1,  
872 this might also happen via the inactivation of other Arf family  
873 members (11, 33). Altogether, our work reveals that in the case  
874 of *S. flexneri* infection, both IpaJ and VirA are necessary to induce  
875 strong recycling inhibition by acting on Arf GTPases and possibly  
876 on Rab GTPases.

877 The targeting of the endosomal compartments by these two  
878 effectors has consequences not only restricted to the surface  
879 receptor recycling, but also to an endocytosis blockage. How IpaJ  
880 and VirA reduce Tf uptake, as well as dynamin 2 and clathrin  
881 recruitment to endocytic sites at the plasma membrane remains  
882 a key question. One hypothesis is that the concerted action of

883 these two effectors on the secretory and recycling pathways will  
884 induce downstream alterations on the endocytic route, as the  
885 intracellular trafficking routes are intimately interlinked. Indeed,  
886 these two *S. flexneri* effectors target two families of proteins  
887 that are key regulators of many intracellular trafficking events,  
888 possibly explaining the endocytosis impairment as an indirect  
889 consequence of their activities on small GTPases. One possibility  
890 suggested by our results is that impairment of exocytosis pathways  
891 by IpaJ and VirA blocks the recruitment of dynamin 2 to the  
892 plasma membrane. Interestingly, this inhibition is also observed  
893 upon BFA treatment, which targets only Arf proteins. However,  
894 the effect of BFA being less strong than *Shigella* infection might  
895 explain why this drug does not significantly decrease Tf endo-  
896 cytosis and further suggests that the combined action of IpaJ  
897 and VirA on Arf and Rab proteins is needed to strongly affect  
898 endocytosis. Moreover, it was also reported that dynamin 2 is  
899 recruited to the budding sites of recycling endosomes, as well as  
900 to the TGN (34, 35), possibly explaining the decreased dynamin  
901 2 recruitment upon *S. flexneri* infection. The bacterium might  
902 also affect endocytosis by targeting actin, an important factor for  
903 dynamin 2 recruitment (36, 37), since it possesses several effec-  
904 tors modulating actin polymerization, such as IpaC, IcsA, and  
905 IpaA (38). In agreement with this, our results demonstrated that  
906 IpaA, a vinculin-binding protein involved in actin reorganization,  
907 partially inhibits endocytosis. Moreover, the plasma membrane  
908 tension, which is regulated by actin polymerization, was shown  
909 to affect endocytosis dynamics in polarized cells (39). Thus, by  
910 targeting actin dynamic regulators, *S. flexneri* might modulate the  
911 plasma membrane tension thereby inhibiting the endocytosis rate  
912 of the host cell.

913 Finally, the global secretion inhibition determined by our  
914 proteomic approach revealed a list of less secreted proteins that  
915 participate in cell polarity establishment and differentiation (40)  
916 and their modulation by *S. flexneri* might perturb the integrity of  
917 the intestinal barrier. Candidates among such proteins are those  
918 regulating cell adhesion, ECM composition and lipid transport. In  
919 addition, the impairment in the secretion of immunomodulators  
920 might affect the host immune response. Moreover, our *in vitro*  
921 data show that IpaJ and VirA subvert the epithelial polarity  
922 and promote multiple invasion events, and we have preliminary  
923 data suggesting that they might regulate intercellular junctions  
924 stability. These results are in total agreement with our *in vivo*  
925 data showing that IpaJ and VirA induce a deeper *S. flexneri*  
926 penetration into the colonic tissue.

927 Overall, our work shows how *S. flexneri* IpaJ and VirA effec-  
928 tors coordinate and modulate the host cell intracellular traffick-  
929 ing, leading to the subversion of the infected cells and tissue that  
930 will result in more efficient bacterial invasion.

## 931 Acknowledgments

932 We are very grateful to Pierre-Henri Commere (PFC, Cytometry Platform  
933 of Institut Pasteur) for technical help with the FACS MoFlo Astrios EQ, Gaëlle  
934 Boncompain and Frank Perez for RUSH reagents, Laurie Pinaud and Claude  
935 Parsot for sharing reagents and helpful discussion and to Katja Brunner  
936 for critical reading of the manuscript. We thank PBI (Imagopole) platform of  
937 Institut Pasteur for microscope maintenance and technical help. This project  
938 was funded by ERC Advanced Grants 232798 and 339579 to PJS, FRM grant  
939 to MLF (SPF20121226366), PTR 22-16 grant to AG, “Région Ile-de-France”  
940 and Fondation pour la Recherche Médicale grants to DL. LS is part of the  
941 Pasteur Paris University (PPU) International PhD Program and has received  
942 funding from the European Union’s Horizon 2020 research and innovation  
943 programme under the Marie Skłodowska-Curie grant agreement No 665807.  
944 **Author contribution** MLF, NS and PJS conceived and designed research. MLF  
945 and VM performed most of the experiments. AG participated on TIRFM  
946 experiments and LS on IL-2R endocytosis and colocalization analysis. GN  
947 performed *in vivo* experiments with MLF. SDL participated on MS post-  
948 analysis. JRR and PS generated *virAipaJ* and *ospC1C2C3* mutant strains,  
949 respectively. VMasson carried out the MS experimental work, GA analyzed  
950 MS data and DL supervised MS and data analysis. MLF and NS wrote the  
951 manuscript with the input of all authors. NS and PJS supervised the project.



953  
954  
955  
956  
957  
958  
959  
960  
961  
962  
963  
964  
965  
966  
967  
968  
969  
970  
971  
972  
973  
974  
975  
976  
977  
978  
979  
980  
981  
982  
983  
984  
985  
986  
987  
988  
989  
990  
991  
992  
993  
994  
995  
996  
997  
998  
999  
1000  
1001  
1002  
1003  
1004  
1005  
1006  
1007  
1008  
1009  
1010  
1011  
1012  
1013  
1014  
1015  
1016  
1017  
1018  
1019  
1020

1. Donaldson JG, Jackson CL (2011) ARF family G proteins and their regulators: roles in membrane transport, development and disease. *Nat Rev Mol Cell Biol* 12(6):362–75.
2. Barr F a (2013) Review series: Rab GTPases and membrane identity: causal or inconsequential? *J Cell Biol* 202(2):191–9.
3. Hutagalung AH, Novick PJ (2011) Role of Rab GTPases in Membrane Traffic and Cell Physiology. *Physiol Rev* 91(1):119–149.
4. Phalipon A, Sansonetti PJ (2007) Shigella 's ways of manipulating the host intestinal innate and adaptive immune system : a tool box for survival ? (September 2006):119–129.
5. Galán JE, Lara-Tejero M, Marlovits TC, Wagner S (2014) Bacterial Type III Secretion Systems: Specialized Nanomachines for Protein Delivery into Target Cells. *Annu Rev Microbiol* 68(1):415–438.
6. Schroeder GN, Hilbi H (2008) Molecular pathogenesis of Shigella spp.: controlling host cell signaling, invasion, and death by type III secretion. *Clin Microbiol Rev* 21(1):134–56.
7. Ashida H, Mimuro H, Sasaki C (2015) Shigella manipulates host immune responses by delivering effector proteins with specific roles. *Front Immunol* 6(MAY). doi:10.3389/fimmu.2015.00219.
8. Parsot C (2009) Shigella type III secretion effectors: how, where, when, for what purposes? *Curr Opin Microbiol* 12(1):110–6.
9. Mounier J, et al. (2012) Shigella Effector IpaB-Induced Cholesterol Relocation Disrupts the Golgi Complex and Recycling Network to Inhibit Host Cell Secretion. *Cell Host Microbe* 12(3):381–9.
10. Burnaevskiy N, et al. (2013) Proteolytic elimination of N-myristoyl modifications by the Shigella virulence factor IpaJ. *Nature* 1:1–17.
11. Burnaevskiy N, Peng T, Reddick LE, Hang HC, Alto NM (2015) Myristoylome profiling reveals a concerted mechanism of ARF GTPase deacylation by the bacterial protease IpaJ. *Mol Cell* 58(1):110–122.
12. Dobbs N, et al. (2015) STING activation by translocation from the ER is associated with infection and autoinflammatory disease. *Cell Host Microbe* 18(2):157–168.
13. Dong N, et al. (2012) Structurally distinct bacterial TBC-like GAPs link Arf GTPase to Rab1 inactivation to counteract host defenses. *Cell* 150(5):1029–1041.
14. Campbell-Volais FX, Sachse M, Sansonetti PJ, Parsot C (2015) Escape of actively secreting shigella flexneri from ATG8/LC3-Positive vacuoles formed during cell-to-cell spread is facilitated by IcsB and VirA. *MBio* 6(3):1–11.
15. Boncompain G, et al. (2012) Synchronization of secretory protein traffic in populations of cells. *Nat Methods* 9(5):493–8.
16. Ong S-E, et al. (2002) Stable Isotope Labeling by Amino Acids in Cell Culture, SILAC, as a Simple and Accurate Approach to Expression Proteomics. *Mol Cell Proteomics* 1(5):376–386.
17. Lippincott-Schwartz J, et al. (1991) Brefeldin A's effects on endosomes, lysosomes, and the TGN suggest a general mechanism for regulating organelle structure and membrane traffic. *Cell* 67(3):601–16.
18. De Figueiredo P, et al. (2001) Inhibition of Transferrin Recycling and Endosome Tubulation by Phospholipase A2Antagonists. *J Biol Chem* 276(50):47361–47370.
19. Robinson MS (2015) Forty Years of Clathrin-coated Vesicles. *Traffic* 16(12):1210–1238.
20. Lamaze C, et al. (2001) Interleukin 2 receptors and detergent-resistant membrane domains define a clathrin-independent endocytic pathway. *Mol Cell* 7(3):661–671.
21. Basquin C, et al. (2015) Membrane protrusion powers clathrin-independent endocytosis of interleukin-2 receptor. *EMBO J* 34(16):1–15.
22. Hunziker W, Andrew Whitney J, Mellman I (1991) Selective inhibition of transcytosis by brefeldin A in MDCK cells. *Cell* 67(3):617–627.
23. Tran Van Nhieu G, Ben-Ze'ev A, Sansonetti PJ (1997) Modulation of bacterial entry into epithelial cells by association between vinculin and the Shigella IpaA invasin. *EMBO J* 16(10):2717–2729.
24. Antony B, et al. (2016) Membrane fission by dynamin: what we know and what we need to know. *EMBO J*. doi:10.15252/embj.201694613.
25. Bertot L, et al. (2018) Quantitative and Statistical Study of the Dynamics of Clathrin-Dependent and -Independent Endocytosis Reveal a Differential Role of EndophilinA2. *Cell Rep* 22(6):1574–1588.
26. Wang E, Pennington JG, Goldenring JR, Hunziker W, Dunn KW (2001) Brefeldin A rapidly disrupts plasma membrane polarity by blocking polar sorting in common endosomes of MDCK cells.
27. Arena ET, et al. (2015) Bioimage analysis of Shigella infection reveals targeting of colonic crypts. *Proc Natl Acad Sci* 112(25):E3282–E3290.
28. Shim D-H, et al. (2007) New Animal Model of Shigellosis in the Guinea Pig: Its Usefulness for Protective Efficacy Studies. *J Immunol* 178(4):2476–2482.
29. Clements A, Stoneham CA, Furniss RCD, Frankel G (2014) Enterohaemorrhagic Escherichia coli inhibits recycling endosome function and trafficking of surface receptors. *Cell Microbiol* 16(11):1693–1705.
30. Grant BD, Donaldson JG (2009) Pathways and mechanisms of endocytic recycling. *Nat Rev Mol Cell Biol* 10(9):597–608.
31. Furniss RCD, Slater S, Frankel G, Clements A (2016) Enterohaemorrhagic E. coli modulates an ARF6:Rab35 signaling axis to prevent recycling endosome maturation during infection. *J Mol Biol* 428(17):3399–3407.
32. Selyunin AS, et al. (2011) The assembly of a GTPase-kinase signalling complex by a bacterial catalytic scaffold. *Nature* 469(7328):107–111.
33. Volpicelli-Daley LA, Li Y, Zhang C, Kahn RA (2005) Isoform-selective Effects of the

#### Bacterial strains

*Shigella flexneri* 5a strain M90T, harboring a streptomycin resistance mutation (41), was used as the WT strain. All the mutants from this study were generated from the WT strain. All the mutant strains used in this study were part of a *S. flexneri* mutant collection (42), except: *ipgD* (43), *virAipA*, *ospE1E2* and *ospC1C2C3*. Tetracycline resistance cassette was removed from *virA* strain to avoid reduction in IcsA protein levels by FLP-FRT recombination using the pCP20 plasmid. Frozen bacterial stocks

34. Depletion of ADP-Ribosylation Factors 1–5 on Membrane Traffic. 16(October):4495–4508.
34. van Dam EM, Stoorvogel W (2002) Dynamin-dependent Transferrin Receptor Recycling by Endosome-derived Clathrin-coated Vesicles. *Mol Biol Cell* 13(1):169–182.
35. Cao H, et al. (2005) Actin and Arf1-dependent recruitment of a cortactin-dynamin complex to the Golgi regulates post-Golgi transport. *Nat Cell Biol*. doi:10.1038/ncb1246.
36. Taylor MJ, Lampe M, Merrifield CJ (2012) A feedback loop between dynamin and actin recruitment during clathrin-mediated endocytosis. *PLoS Biol*. doi:10.1371/journal.pbio.1001302.
37. Grassart A, et al. (2014) Actin and dynamin2 dynamics and interplay during clathrin-mediated endocytosis. *J Cell Biol*. doi:10.1083/jcb.201403041.
38. Valencia-Gallardo CM, Carayol N, Tran Van Nhieu G (2015) Cytoskeletal mechanics during Shigella invasion and dissemination in epithelial cells. *Cell Microbiol* 17(2):174–182.
39. Boulant S, Kural C, Zeeh JC, Ubelmann F, Kirchhausen T (2011) Actin dynamics counteract membrane tension during clathrin-mediated endocytosis. *Nat Cell Biol*. doi:10.1038/ncb2307.
40. García-Lorenzo A, Rodríguez-Piñero AM, Rodríguez-Berrocal FJ, de la Cadena MP, Martínez-Zorzano VS (2012) Changes on the Caco-2 secretome through differentiation analyzed by 2-D differential in-gel electrophoresis (DIGE). *Int J Mol Sci* 13(11):14401–14420.
41. Allaoui A, Sansonetti PJ, Parsot C (1992) MxiJ, a lipoprotein involved in secretion of Shigella Ipa invasins, is homologous to YscJ, a secretion factor of the Yersinia Yop proteins. *J Bacteriol* 174(23):7661–7669.
42. Sidik S, et al. (2014) A Shigella flexneri Virulence Plasmid Encoded Factor Controls Production of Outer Membrane Vesicles. *G3&#amp;#273; Genes|Genomes|Genetics* 4(12):2493–2503.
43. Allaoui A, Menard R, Sansonetti PJ, Parsot C (1993) Characterization of the Shigella flexneri ipgD and ipgF genes, which are located in the proximal part of the mxi locus. *Infect Immun* 61(5):1707–1714.
44. Grassart A, Dujeancourt A, Lazarow PB, Dautry-Varsat A, Sauvonnnet N (2008) Clathrin-independent endocytosis used by the IL-2 receptor is regulated by Rac1, Pak1 and Pak2. *EMBO Rep* 9(4):356–362.
45. Fourriere L, Divoux S, Roceri M, Perez F, Boncompain G (2016) Microtubule-independent secretion requires functional maturation of Golgi elements. *J Cell Sci* 129(17):3238–3250.
46. Labigne-Roussel AF, Lark D, Schoolnik G, Falkow S (1984) Cloning and expression of an afimbrial adhesin (AFA-I) responsible for P blood group-independent, mannose-resistant hemagglutination from a pylonephritic Escherichia coli strain. *Infect Immun*.
47. Valdivia RH, Falkow S (1996) Bacterial genetics by flow cytometry: Rapid isolation of Salmonella typhimurium acid-inducible promoters by differential fluorescence induction. *Mol Microbiol* 22(2):367–378.
48. Sörensen M, et al. (2003) Rapidly maturing red fluorescent protein variants with strongly enhanced brightness in bacteria. *FEBS Lett* 552(2–3):110–114.
49. Campbell-Volais F-X, et al. (2014) A fluorescent reporter reveals on/off regulation of the Shigella type III secretion apparatus during entry and cell-to-cell spread. *Cell Host Microbe* 15(2):177–89.
50. Poulet P, Carpentier S, Barillot E (2007) myProMS, a web server for management and validation of mass spectrometry-based proteomic data. *Proteomics* 7(15):2553–2556.
51. Valot B, Langella O, Nano E, Zivy M (2011) MassChroQ: A versatile tool for mass spectrometry quantification. *Proteomics* 11(17):3572–3577.
52. Ritchie M, et al. (2015) limma powers differential expression analyses for RNA-sequencing and microarray studies. *Nucleic Acids Res* 43(7):e47.
53. Benjamini Y, Hochberg Y, Benjamini Y, and Hochberg Y (1995) Controlling the false discovery rate: a practical and powerful approach to multiple testing. *J R Stat Soc Ser B Methodol* 57(1):289–300.
54. Vizcaino JA, et al. (2016) 2016 update of the PRIDE database and its related tools. *Nucleic Acids Res* 44(D1):D447–D456.
55. Kowal J, et al. (2016) Proteomic comparison defines novel markers to characterize heterogeneous populations of extracellular vesicle subtypes. *Proc Natl Acad Sci* 113(8):E968–E977.
56. Petersen TN, Brunak S, Von Heijne G, Nielsen H (2011) SignalP 4.0: Discriminating signal peptides from transmembrane regions. *Nat Methods*. doi:10.1038/nmeth.1701.
57. Bendtsen JD, Jensen LJ, Blom N, Von Heijne G, Brunak S (2004) Feature-based prediction of non-classical and leaderless protein secretion. *Protein Eng Des Sel*. doi:10.1093/protein/gzh037.
58. Ashburner M, et al. (2000) Gene ontology: Tool for the unification of biology. *Nat Genet* 25(1):25–29.
59. Thomas PD, et al. (2003) PANTHER: A library of protein families and subfamilies indexed by function. *Genome Res*. doi:10.1101/gr.772403.
60. Schindelin J, et al. (2012) Fiji: An Open-Source Platform for Biological- Image Analysis. *Nat Methods* 9(June 2012):676–682.
61. De Chaumont F, et al. (2012) Icy: An open bioimage informatics platform for extended reproducible research. *Nat Methods*. doi:10.1038/nmeth.2075.
62. Lagache T, et al. (2018) Mapping molecular assemblies with fluorescence microscopy and object-based spatial statistics. *Nat Commun* 9(1):102–108.

#### Methods

were streaked onto trypticase soy agar (TSA) plates containing 0.1% (w/v) Congo red (CR) and grown at 37 °C overnight. Plates were kept at 4 °C for up to two weeks.

#### Cell lines

Hep2 cells (HeLa derivative) and its derivatives expressing the  $\beta$ -chain of IL-2R, Hep2 $\beta$ , were grown in DMEM 1 g/L (Gibco™) supplemented with 10% heat-inactivated fetal calf serum (HI-FCS, Eurobio) at 5% CO<sub>2</sub> at 37° C (44), in the presence of 1 mg/mL G418 (Sigma) for Hep2 $\beta$  cells. CRISPR-Cas9 genome edited Hep2 $\beta$  Dnm2-

1021  
1022  
1023  
1024  
1025  
1026  
1027  
1028  
1029  
1030  
1031  
1032  
1033  
1034  
1035  
1036  
1037  
1038  
1039  
1040  
1041  
1042  
1043  
1044  
1045  
1046  
1047  
1048  
1049  
1050  
1051  
1052  
1053  
1054  
1055  
1056  
1057  
1058  
1059  
1060  
1061  
1062  
1063  
1064  
1065  
1066  
1067  
1068  
1069  
1070  
1071  
1072  
1073  
1074  
1075  
1076  
1077  
1078  
1079  
1080  
1081  
1082  
1083  
1084  
1085  
1086  
1087  
1088

1089 GFP and Hep2β CLC-GFP cells (25), and the RUSH stable HeLa cell line expressing  
1090 the ER molecular hook Streptavidin-KDEL and the cargo SBP-EGFP-TNFα (45) were  
1091 described previously. Hep2 and HeLa cells are non-polarized cell, and were always  
1092 cultured to 70% confluence prior to infection experiments. Caco-2/TC7 cells (a clone  
1093 of Caco-2 cells, human colorectal adenocarcinoma origin) were grown in DMEM  
1094 1 g/L supplemented with 20% HI-FCS, GlutaMAX™ and non-essential amino acids  
1095 (Gibco™). For complete polarization and differentiation of Caco-2/TC7 cells, 2x10<sup>5</sup>  
1096 cells/cm<sup>2</sup> cells were seeded into 12-well or 6-well Transwell inserts (pore size 0.4  
1097 μm, Corning) and cultured for 18-21 days at 10% CO<sub>2</sub> at 37° C; fresh media was  
1098 added triweekly, except for plaque assay experiments, where cells were cultured  
1099 on plastic 6-well plates. Transepithelial electrical resistance (TEER) was measured  
1100 using a Millicell-ERS Volt-ohm meter (Millipore). Dextran permeability was assessed  
1101 by adding 70 kDa FITC-Dextran 200 μg/mL (Sigma) in Ringer's buffer to the apical  
1102 compartment of Transwell inserts (uninfected or infected in Ringer's solution: 155  
1103 mM NaCl, 3 mM KCl, 3 mM NaH<sub>2</sub>PO<sub>4</sub>, 5 mM Hepes 10 mM Glucose, pH 7.0, with 2  
1104 mM CaCl<sub>2</sub>, 1 mM MgCl<sub>2</sub>) after a 15 min preincubation in Ringer's buffer or in calcium-  
1105 free Ringer's (containing 10 mM glucose). Fluorescence pass-through to the basal  
1106 compartment medium was measured with an Infinite M200 Pro multimode plate-  
1107 reader (TECAN). Lactate dehydrogenase (LDH) was quantified with the CytoTox 96®  
1108 Non-Radioactive Cytotoxicity Assay (Promega).

**Plasmids**  
1109 Bacteria transformed with plasmids coding for the *Escherichia coli* AfaE adhesin (46),  
1110 or GFP (pFPV 25.1) (47), dsRed (48) or mCherry fluorescent proteins, were used as  
1111 indicated. pTRIO-mCherry plasmid was generated by inserting mCherry CDS in *Xmal*-  
1112 *NheI* sites of pTRIO plasmid, which is the basic backbone of the pTSAR plasmids series  
1113 (49). The CDS of *ipaJ* was cloned through *EcoRI*-*Bam*HI into pSU2.1tt plasmid (49),  
1114 giving the pSU2.1tt-*ipaJ*-Myc plasmid. The catalytic site variant was generated by  
1115 PCR-based mutagenesis introducing the C64A mutation into *ipaJ* (plasmid pSU2.1tt-  
1116 *ipaJ*-C64A-Myc). *ipaJ* and *virAipaJ* mutant strains were complemented with pSU2.1tt-  
1117 *ipaJ*-Myc or pSU2.1tt-*ipaJ*-C64A-Myc plasmids. pSU2.1tt-*VirA*-Myc or pSU2.1tt-*VirA*-  
1118 RQ-Myc plasmids (14) were used to complement *virAipaJ* or *virA* strains. For the  
1119 ectopic expression of GFP-*VirA*, GFP-*ipaJ* and their mutated variants in mammalian  
1120 cells, the CDS of *ipaJ* and *virA* were cloned through *Hind*III-*Kpn*I into pEGFP-C1  
1121 plasmid.

**Antibodies and reagents**  
1122 The following primary antibodies were used: rabbit anti-*S. flexneri* 5a M90T LPS  
1123 1:300, mouse anti-GM130 1:200 (BD, #610823), rabbit anti-GM130 1:100 (Abcam,  
1124 ab52649), mouse anti-GFP DyLight 680 1:1000 (Rockland, #600-144-215), mouse anti-  
1125 ERGIC53 1:100 (Sigma, SAB4200585), rabbit anti-Sec24b 1:100 (D7D65) (Cell Signaling  
1126 Technology, #12042), sheep anti-TGN46 1:100 (Bio-Rad, AHP500GT), purified mouse  
1127 mAb OKT9 (anti-TfR) 1:100, goat anti-dynamin-2 1:500 (Santa Cruz, sc-6400), rabbit  
1128 anti-clathrin LCA (H-55) 1:500 (Santa Cruz, sc-28276), rabbit anti-GFP 1:1000 (Rock-  
1129 land, #600-401-215), rabbit anti-actin 1:5000 (Sigma, A2066), chicken anti-GFP 1:1000  
1130 (Abcam, ab13970). All the secondary antibodies were from all from Molecular Probes  
1131 and used at 1:500 dilution. FITC-Dextran 70 (Sigma, #46945), Dapi 1 μg/mL (Sigma).  
1132 Phalloidin-AF647 1:100 (A22287, Molecular Probes). Brefeldin A (Sigma, B7651) was  
1133 used at 1 μg/mL.

**Bacterial infections of cultured cells**  
1134 Hep2 and Hep2β cells were plated the day before the experiment onto 12-mm  
1135 coverslips at a density of 0.4x10<sup>5</sup> cells/cm<sup>2</sup> for immunofluorescence, or on glass  
1136 bottom dishes (Mattek) for total internal reflection fluorescence (TIRF) microscopy  
1137 experiments, and at a density of 0.4x10<sup>5</sup> cells/cm<sup>2</sup> on 6-well plates for flow cytometry  
1138 (FC) or western blot experiments. Bacterial cultures were prepared by picking a  
1139 single colony from each strain from TSA-CR plates and grown in 8 mL of trypticase  
1140 soy broth (TSB) supplemented with the appropriate antibiotics (ampicillin 100 μg/mL,  
1141 chloramphenicol 10 μg/mL) in a shaking incubator overnight at 30 °C. Bacteria were  
1142 sub-cultured in fresh 8 mL TSB at 37° C until OD<sub>600</sub> 0.8 – 1.0, pelleted, washed in  
1143 PBS and coated with poly-L-lysine (mol wt 70,000 – 100,000, Sigma) 10 μg/mL in  
1144 PBS for 10 min, washed twice with PBS and resuspended in the infection medium  
1145 (DMEM supplemented with 20 mM Hepes) to the adequate multiplicity of infection  
1146 (MOI). Coated bacteria were added to the cells and allowed to adhere for 15 min at  
1147 room temperature (RT), and then incubated at 37° C in a CO<sub>2</sub> incubator or in a water  
1148 bath when short time of infection or short kinetics were performed. For infections of  
1149 Caco-2/TC7 cells grown in transwell filters, AfaE-expressing strains were cultured as  
1150 described, pelleted, washed with PBS and resuspended in infection medium to the  
1151 adequate MOI. Apical and basal chambers were washed twice with warm DMEM-  
1152 Hepes and bacteria were added to the apical chamber at a MOI = 75, incubated for  
1153 15 min at RT and switched to a 37 °C CO<sub>2</sub> incubator. After 30 min, the medium was  
1154 aspirated and replaced for fresh DMEM-Hepes supplemented with gentamicin 50  
1155 μg/mL and incubated for the indicated additional time.

For plaque assays, Caco-2/TC7 cell monolayers were cultured on plastic 6-well plates  
1156 for 3 weeks, infected at a MOI of 5 for 2 hours, washed and followed by the addition  
1157 of a 0.5% agarose overlay containing 50 μg/mL gentamicin in culture medium. 48  
1158 hours later, cells were fixed with ethanol and stained with Giemsa R solution. Plaque  
1159 sizes were quantified using Fiji (Image J) software.

**RUSH assay to assess anterograde trafficking**  
1160 RUSH stable HeLa cell line expressing the ER molecular hook Streptavidin-KDEL and  
1161 the cargo SBP-EGFP-TNFα (45) were uninfected or infected with the indicated *S.*  
1162 *flexneri* strain expressing mCherry fluorescent protein. After 15 min at RT and 45  
1163 min at 37 °C, the medium was replaced by medium containing 40 μM of biotin  
1164 (Sigma) to initiate the cargo transport from the ER and incubated at 37 °C for  
1165 additional 60 min. Cells were washed with ice-cold PBS, fixed in PFA 4%-PBS for  
1166 20 min on ice and stained for 1 hour at RT with an anti-GFP DyLight 680 antibody  
1167 (Rockland) to detect the surface-arrived SBP-EGFP-TNFα. After harvesting, surface

anti-GFP DyLight 680 fluorescence was measured by FC (MoFlo Astrios EQ, Beckman)  
1168 in the infected population of cells (mCherry positive). Results are the mean expressed  
1169 as the percentage of total (uninfected or infected) cells expressing the RUSH cargo  
1170 at their surface. Alternatively, cells grown on coverslips were infected as before and  
1171 subsequent immunofluorescences were performed as indicated in the figures.

**SILAC labeling, infections, sample collection and preparation**  
1172 Human Caco-2/TC7 cells were cultured for 6 passages in SILAC DMEM flex media  
1173 deficient for L-arginine and L-lysine (Gibco) with 20% heat inactivated dialyzed FBS  
1174 (dFBS) (Thermo Fischer), 1 g/L glucose (Sigma), GlutaMAX 1X, non essential amino  
1175 acids, 10 U/mL penicillin/streptomycin (all from Gibco) supplemented with either  
1176 13C6, 15N4 L-Arginine-HCl and 13C6, 15N2 L-Lysine-2HCl (Heavy media) or with 13C6  
1177 L-Arginine-HCl and 4,4,5,5-D4 L-Lysine-2HCl (Medium media) (arginine at 84mg/mL  
1178 and lysine at 146 mg/mL, Thermo Fisher Scientific). The stable isotope labeling was  
1179 confirmed by LC-MS/MS after protein in-gel separation and digestion of blue bands.  
1180 Labeled cells were seeded on 6-well Transwell inserts and cultured for 21 days in  
1181 Heavy or Medium SILAC medium changing the medium 3 times per week.  
1182 For secretome collection, 24 hours before infections cells were washed with DMEM  
1183 for SILAC with 20 mM Hepes and medium was replaced with either Medium or Heavy  
1184 SILAC media but containing 2% dFBS. Cells were uninfected or infected with AfaE-  
1185 expressing WT or *virAipaJ* strains. To that end, apical and basal chambers of Transwell  
1186 inserts were washed 3 times with DMEM for SILAC/Hepes, Medium SILAC medium  
1187 was added to uninfected cells, and bacteria were added in the apical chamber at a  
1188 MOI 75 in Heavy SILAC medium without FBS or antibiotics. After 15 min at RT and 30  
1189 min at 37° C, cells were washed 3 times with DMEM for SILAC/Hepes, 1.5 mL of FBS-  
1190 free Medium or Heavy SILAC media with 50 μg/mL gentamicin were added at either  
1191 apical or basal Transwell chambers, and cells were further incubated at 37° C for 4 ½  
1192 hours. Apical and basal secretomes were collected (total volume: 3.6 mL/condition),  
1193 UI and infected samples mixed in a 1:1 ratio, centrifuged (200 x g, 5 min), filtered  
1194 with 0.22 μm syringe filters (Minisart, Sartorius Stedim Biotech S.A.) and snap-frozen  
1195 in liquid N<sub>2</sub>. For proteome analysis, cells were lysed in RIPA buffer containing  
1196 protease inhibition cocktail and samples were mixed at a protein stoichiometry ratio  
1197 of UI:infected 1:1. Samples were kept at -80° C until use. Before trypsin digestion,  
1198 uninfected and infected secretomes mixing at a 1:1 ratio was done according to cell  
1199 number in Transwells from which the secretome was prepared (total volume = 3.6  
1200 mL), and then concentrated to 500 μL on Amicon Ultra-15, 10000 molecular weight  
1201 cutoff centrifugation filter units (Millipore). For the filter-aided sample preparation  
1202 protocol (FASP), a total of 60 mg of urea and 16 μL of M dithiothreitol were added  
1203 to 500 μL of concentrated secretome, the solution was mixed on a Nanosep (10 kDa,  
1204 Pall) device, and was incubated at 57 °C for 15 min. The mixture was spun down  
1205 and was washed two times with 500 μL of 2 M urea in 0.1 Tris/HCl pH 8.5. A total of  
1206 100 μL of 0.05 M iodoacetamide was added and was incubated for 30 min at RT in  
1207 the dark. Two washes with 25 mM ammonium bicarbonate were performed and the  
1208 secretome was digested with 5 μg of trypsin / LysC (Promega) for 4 hours at 37 °C.  
1209 The digested peptides were collected by centrifugation, and the filtrate was dried in  
1210 a vacuum concentrator at room temperature and was re-dissolved in solvent A (2%  
1211 acetonitrile, 0.1 % formic acid). Peptides were then subjected to LC/MS analysis.  
1212 For proteome analysis, mixed proteins lysates were separated on 10% SDS-PAGE (Thermo  
1213 Fisher Scientific) and were digested in-gel with trypsin / LysC (Promega) as described  
1214 in standard protocols. Extracted peptides were dried in a vacuum concentrator at  
1215 room temperature and were re-dissolved in solvent A (2% MeCN, 0.1% HCO<sub>2</sub>H)  
1216 before LC/MS analysis.

**LC-MS/MS analysis**  
1217 For the analysis of cell lysates, peptides were separated by reverse-phase chromatog-  
1218 raphy by using an UltiMate 3000 RSLCnano system coupled to an Orbitrap Fusion  
1219 mass spectrometer (Q-OT-qIT, Thermo Fisher Scientific). Samples were loaded on a  
1220 nanoViper C18 μ-precolumn (75μm x 2 cm, Acclaim PepMap, Thermo Scientific) at  
1221 5 μL/min of solvent A. After a desalting of 8 min, the precolumn was switched on  
1222 the C18 column (75μm x 50 cm; 3 μm, 100Å, Acclaim PepMap, Thermo Scientific)  
1223 equilibrated in solvent A. Bound peptides were eluted using a 168 min four step  
1224 linear gradient (from 5 to 6% (v/v) in one min, 6 to 9% in 18 min, 9 to 30% in 132  
1225 min and 30 to 40% in 9 min) of solvent B (100% MeCN, 0.085% HCO<sub>2</sub>H) at 60° C and  
1226 a 300 nL/min flow rate.

For the analysis of secretome samples, peptides were loaded on a C18 μ-precolumn  
1227 (Thermo Scientific) at 20 μL/min in solvent A. After a desalting step for 3 min,  
1228 the precolumn was switched on the C18 column (Thermo Scientific) equilibrated in  
1229 solvent A and peptide were eluted with a 215 minute two step linear gradient of  
1230 solvent B (from 5 to 20% (v/v) in 147 min and 20 to 40% in 65 min).  
1231 We acquired Survey MS scans at a resolution set to a value of 120,000, with a mass  
1232 range of m/z 400–1500 and a 4 × 10<sup>5</sup> ion count target. Tandem MS was performed by  
1233 isolation at 1.6 Th with the quadrupole, HCD fragmentation with normalized collision  
1234 energy of 28, and rapid scan MS analysis in the ion trap. The MS<sup>2</sup> ion count target was  
1235 set to 1 × 10<sup>4</sup> and only those precursors with charge state from 2 to 7 were sampled  
1236 for MS<sup>2</sup> acquisition. The instrument was run in top speed mode with 3 s cycles.

**LC-MS/MS Data Processing and Protein Identification**  
1237 Data were acquired using the Xcalibur software (v 3.0) and the resulting spectra  
1238 were interrogated by Sequest HT through Thermo Scientific Proteome Discoverer  
1239 (v 2.1) with the SwissProt human database (012016). The mass tolerances in MS and  
1240 MS/MS were set to 10 ppm and 0.6 Da, respectively. We set carbamidomethyl cysteine,  
1241 oxidation of methionine, N-terminal acetylation, heavy <sup>13</sup>C<sub>6</sub><sup>15</sup>N<sub>2</sub>-Lysine (Lys8) and  
1242 <sup>13</sup>C<sub>6</sub><sup>15</sup>N<sub>4</sub>-Arginine (Arg10), medium <sup>2</sup>H<sub>4</sub>-Lysine (Lys4) and <sup>13</sup>C<sub>6</sub>-Arginine (Arg6) as  
1243 variable modifications. We set specificity of Trypsin digestion and allowed 2 missed  
1244 cleavage sites.

The resulting files were further processed by using myProMS (v 3.5) (50). The Sequest  
1245 HT target and decoy search result were validated at 1% false discovery rate (FDR)  
1246 1222

1225 with Percolator. For SILAC-based protein quantification, peptides XICs (Extracted  
1226 Ion Chromatograms) were retrieved from Thermo Scientific Proteome Discoverer or  
1227 computed with MassChroQ version 1.2.1 (51). Global MAD normalization or not was  
1228 applied on the total signal to correct the XICs for each biological replicate. Protein  
1229 ratios were computed as the geometrical mean of related peptides. To estimate ratio  
1230 significance, a t-test was performed with the R package limma (52) and the false  
1231 discovery rate has been controlled thanks to the Benjamini-Hochberg procedure (53)  
1232 with a threshold set to 0.05.  
1233 The mass spectrometry proteomics data have been deposited to the ProteomeX-  
1234 change Consortium via the PRIDE (54) partner repository with the dataset identifier  
1235 PXD012291.  
1236 **Bioinformatics analysis**  
1237 myProMS (v 3.5) (50) was used to analyze SILAC results. Proteins from infected  
1238 secretomes were considered as differentially secreted from uninfected secretomes  
1239 when showing a fold change above or less than 2,  $p < 0.05$  and at least 3 detected  
1240 peptides. Fold change-based gene ontology (GO) enrichment analysis was performed  
1241 as in (55). SignalP 4.0 (56) was used to determine which proteins contained a signal  
1242 peptide (predicted or confirmed). SecretomeP 2.0 (57) was used to detect non-  
1243 conventional secretion; proteins above a cut-off of 0.5 were considered as secreted  
1244 proteins. GO terms (58) were extracted from PANTHER (59) and UniprotKB.  
1245 **Transferrin (Tf) recycling and endocytosis**  
1246 For Tf recycling experiments, Hep2 cells cultured in 6-well plates were incubated at  
1247 RT with DMEM-Hepes (UI) or the indicated bacterial strains expressing GFP or dsRed  
1248 proteins at a MOI of 100. After 15 minutes of infection, human Tf coupled to Alexa  
1249 Fluor 647 (Tf-AF647) (Invitrogen) was added at 0.5  $\mu\text{g}/\text{mL}$  in DMEM-Hepes-0.1% BSA  
1250 at 37 °C. After 30 min of incubation to allow Tf-AF647 endocytosis, surface Tf-AF647  
1251 was removed by treating cells with ice-cold sodium acetate 20 mM pH 3.0 for 3  
1252 minutes at 4 °C before neutralization with DMEM-HEPES pH 10. Cells were incubated  
1253 back at 37 °C in DMEM-Hepes-0.1% BSA supplemented with 50  $\mu\text{g}/\text{mL}$  of human non-  
1254 fluorescent holo-transferrin to perform a time course. Cells were scraped gently and  
1255 transferred into ice-cold PBS for flow cytometry (FC) analysis.  
1256 For Tf endocytosis, Hep2 cells were uninfected or infected with GFP-expressing  
1257 relevant strains as previously described. After 60 min of infection at MOI 10, cells  
1258 were washed twice with warm DMEM-Hepes and incubated for additional 30 min in  
1259 the same medium containing 0.1% BSA and gentamicin 50  $\mu\text{g}/\text{mL}$  to kill extracellular  
1260 bacteria. Tf uptake time-course was performed by incubating cells in a water  
1261 bath at 37 °C with DMEM-Hepes-0.1% BSA in the presence of 0.5  $\mu\text{g}/\text{mL}$  Tf-AF647  
1262 for different time points, followed by an acid stripping of remaining membrane  
1263 associated Tf-AF647.  
1264 To measure surface TFR levels, UI or infected cells were incubated at 4 °C in the  
1265 presence of Tf-AF647 for 30 minutes. Cells were acid washed or untreated, and the  
1266 total surface Tf-AF647 fluorescence was quantified by FC.  
1267 Where indicated, cells were transfected with the relevant plasmids the day before  
1268 the Tf recycling or endocytosis experiments by electroporation (10  $\mu\text{g}$  DNA/4.5x10<sup>6</sup>  
1269 cells) or using Lipofectamine 3000 (Thermo Fischer Scientific).  
1270 The Geometrical Mean Fluorescence of intracellular Tf-AF647 was measured in gated  
1271 living cells (using Dapi or Live/Dead Fixable Violet Cell Stain Kit, L34955, Molecular  
1272 Probes) by FC in a BD FACSCanto II Flow Cytometer (BD Biosciences) or an Attune  
1273 NxT Flow Cytometer (Thermo Fischer Scientific). Tf recycling results were expressed  
1274 as the percentage of the remaining intracellular Tf-AF647 at each time point respect  
1275 to time 0 of recycling. Tf recycling rate was determined from the slope of ln2 data  
1276 during the first 30 minutes of kinetics. Tf endocytosis results were expressed as Tf  
1277 endocytosis rate, calculated as the internal Tf-AF647 fluorescence over time, during  
1278 the first 10 minutes of kinetics.  
1279 **IL-2R $\beta$  endocytosis**  
1280 Hep2 $\beta$  cells seeded on 12-mm coverslips were uninfected or infected with GFP-  
1281 expressing bacteria. After 90 min of infection, a time-course of IL-2R $\beta$  endocytosis  
1282 was performed by incubating cells with an anti-IL-2R $\beta$  antibody (mouse Ab 561)  
1283 conjugated to Cy3 (1:1000) (44) at 37 °C for different time points. Cells were fixed,  
1284 permeabilized and stained with HCS CellMask Blue Stain (Molecular Probes) and  
1285 Phalloidin-AF647 or Tf-AF647. Imaging was performed by TIRF microscopy. IL-2R $\beta$   
1286 endocytosis was quantified with ICY software as described in (21).  
1287 **Animals, infections and sample preparation**  
1288 Guinea pigs were infected according to previously described protocols (27, 28).  
1289 Female specific pathogen-free Hartley guinea pigs (120–250 g) were purchased from  
1290 Charles River Laboratories, maintained in animal care facilities of Institut Pasteur,  
1291 and provided with food and water *ad libitum*. Animal experiments were carried out  
1292 under approval by the "Use Committee of Institut Pasteur and by the French Ministry  
1293 of Agriculture no. 2013-0113". Briefly, animals were anesthetized intraperitoneally  
1294 using a mixture of ketamine (100 mg/kg; Merial) and xylazine hydrochloride (10  
1295 mg/kg; Bayer) before intrarectal inoculation of *S. flexneri* strains at 5x10<sup>10</sup> cfu per  
1296 200  $\mu\text{L}$ . Animals were sacrificed at 4 and 8 hours postchallenge. The distal 10 cm of  
1297 colon was harvested and fixed overnight in 4% (vol/vol) PFA in PBS, and incubated  
1298 in PBS-glycine (100 mM) for 30 min to quench the PFA. Tissues were then immersed  
1299 successively in 15% and 30% (wt/vol) sucrose at 4 °C overnight. Tissues were cut and  
1300 embedded in Tissue-Tek OCT compound (Sakura) using a flash-freeze protocol and  
1301 frozen at -80 °C.

1302 **Immunofluorescence**  
1303 Hep2 and Hep2 $\beta$  cells were fixed in PFA 4% sucrose 4% in PBS for 20 min and  
1304 quenched with NH<sub>4</sub>Cl 50 mM for 10 min. Permeabilization, blocking, incubations  
1305 and washes were done with PBS BSA 0.1% saponin 0.05%. Polarized Caco-2/Tc7 cells  
1306 were washed, fixed and quenched preparing solutions in PBS with Ca<sup>2+</sup> and Mg<sup>2+</sup>  
1307 (Gibco). Permeabilization was done in PBS Ca<sup>2+</sup> Mg<sup>2+</sup> gelatin 0.2%, saponin 0.075%  
1308 for 1 hour at RT, primary antibodies incubated for 90 min at RT or overnight at 4  
1309 °C, secondary antibodies 1 hour at RT, together with Dapi 1  $\mu\text{g}/\text{mL}$  and Phalloidin  
1310 coupled to AlexaFluor (Molecular Probes) if indicated.  
1311 For tissue sections, immunofluorescence samples were prepared as follows: 10  $\mu\text{m}$ -  
1312 thick transversal colon sections were permeabilized in PBS 0.5% Triton X-100 for 30  
1313 min, blocked in PBS 1% BSA for 30 min at RT and incubated overnight at 4 °C with the  
1314 indicated primary antibodies, together with Phalloidin AlexaFluor 647 (1:100) diluted  
1315 in PBS, 0.1% Triton X-100, 1% BSA. Sections were then washed with PBS and stained  
1316 for 1–2 hours at RT with AlexaFluor 568 goat anti-mouse or anti-rabbit (A11031 and  
1317 A11036; Molecular Probes), followed by incubation with Dapi (1  $\mu\text{g}/\text{mL}$ ) for 10 min  
1318 at RT. Samples were washed with PBS before mounting.  
1319 ProLong Gold Antifade (Molecular Probes) was used as mounting medium.  
1320 **Image acquisition**  
1321 The following equipment was used for image acquisition: a LSM700 inverted laser  
1322 scanning confocal microscope (Zeiss), with a 40x/1.4 Oil immersion or a 63x/1.4 Oil  
1323 immersion objective (Zeiss); an Axio Observer.Z1 microscope (Zeiss) equipped with a  
1324 swept field confocal Opterra system (Bruker) and an Evolve 512 Delta EMCCD camera  
1325 (Photometrics), using a 63x PlanAPO-CHROMAT oil immersion/1.4 NA objective  
1326 (Zeiss); a slide scanner Axio Scan.Z1 (Zeiss), using a 40x dry objective; an inverted  
1327 confocal microscope LSM 780 Elyra PS.1 (Zeiss), using an alpha Plan Apo 100X/1.46  
1328 NA oil objective (Zeiss) (TIRF imaging).  
1329 **Image analysis and quantification**  
1330 Microscopy images were processed and quantified with Fiji (ImageJ) (60), ICY soft-  
1331 ware (61) (<http://icy.bioimageanalysis.org>) or Zen (Zeiss). Colocalization quantifica-  
1332 tion was performed on confocal images using the Statistical Object Distance Analysis  
1333 (SODA) plugin in ICY software described in (62). IL-2R $\beta$  endocytosis was quantified  
1334 with ICY software using "HK-Means" and "Active Contours" plugins to automatically  
1335 detect cell boundaries and "Spot Detector" plugin to measure the number of the IL-  
1336 2R $\beta$  spots within the detected cells. The total intensity of IL-2R $\beta$  spots was normalized  
1337 to the mean value of the uninfected conditions. Quantification of Dnm2 or CLC  
1338 density at plasma membrane from TIRF images was performed using ICY "Spot  
1339 detector" plugin to quantify the number of spot per cell area. Quantification of Tf-  
1340 A647 uptake by Caco-2/Tc7 cells was performed with Fiji, by quantifying the total  
1341 fluorescence per cell from 10 slices of 0.8  $\mu\text{m}$  from a z-stack. Tissue images were  
1342 acquired with 40X objectives and subsequent stitching was performed using Zen  
1343 software to build the mosaic images. Quantification of bacteria depth penetration  
1344 into the intestinal mucosa was done from images illustrated in Fig. S4C with Fiji,  
1345 by measuring the maximum bacterial distance of penetration from the epithelium  
1346 surface, respect to the total mucosal thickness.  
1347 **Data presentation and statistical analysis**  
1348 Prism 6.0 (GraphPad Software, Inc.) was used to perform statistical analysis. Results  
1349 are represented as mean  $\pm$  SD, except otherwise indicated. The following statistical  
1350 tests were used: Welch's t-test performed as unpaired two-tailed analysis; one-way  
1351 ANOVA followed by Dunnett's or Tukey's *post-hoc* multiple comparison tests; Mann-  
1352 Whitney; Kruskal-Wallis followed by Dunn's *post-hoc* test.  $P < 0.05$  was considered  
1353 significant for all analyses.  
1354 Fiji and Zen (Zeiss) were used to process microscopy images. Inkscape software  
1355 (<http://www.inkscape.org/>) was used for assembling figures.